



Contents lists available at ScienceDirect

Journal of Computational and Applied Mathematics

journal homepage: www.elsevier.com/locate/cam

Resonance dynamics of kinks in the sine-Gordon model with impurity, external force and damping

Evgenii G. Ekomasov^{a,b}, Azamat M. Gumerov^{a,*}, Roman V. Kudryavtsev^a^a Bashkir State University, 450076, Z. Validi St., 32, Ufa, Russia^b National Research South Ural State University, 454080, Lenina prospect 76, Chelyabinsk, Russia

ARTICLE INFO

Article history:

Received 26 September 2015

Received in revised form 10 April 2016

MSC:

35C08

35Q51

65M06

Keywords:

Modified sine-Gordon equation

Impurity

Kink

Resonance dynamics

ABSTRACT

We study the resonance dynamics of the sine-Gordon equation kinks with a point impurity. We consider the possibility of localized nonlinear waves generation on the impurities. By using analytical and numerical methods we show that the damping and external force counteract the development of kink resonant reflection from the attracting impurity. However, the underlying cause – a resonant energy exchange between solitons – still occurs.

© 2016 Elsevier B.V. All rights reserved.

1. Introduction

With the help of soliton dynamics one currently describes more and more physical applications in hydrodynamics, condensed matter physics, field theory, etc. (see [1–3]). The present paper deals with the modified sine-Gordon equation (MSGE)

$$u_{tt} - u_{xx} + \sin u = \Phi, \quad (1)$$

where summand Φ contains perturbations of problem. MSGE plays an important role in a number of physical problems: the domain walls in magnetics, dislocations in crystals, fluxons in Josephson junctions and crossings, etc. (see [4]). In many cases, the behavior of solitons can be described in terms of a point particle model, then their temporal evolution will be subject to the simple differential equations (see e.g. [1,2,4]). Accounting the perturbation effect leads to a significant change in the structure of solitons, which have to be described as deformable quasiparticles (see [1,2,4,5]). At the same time, the solitons internal degrees of freedom are excited, and they can play a decisive role in some physical effects. Inner modes include translational and related to long-lived oscillations of the soliton width oscillatory mode (see [1,2]).

If the study of the small perturbations influence on the MSGE solutions can be carried out by a well-developed perturbation theory for solitons [1,2,5], then the influence of large perturbations in the general case can be carried out only with the help of numerical methods (see e.g. [6–8]). Thus far quite a number of methods for numerical solving of such equations

* Corresponding author.

E-mail addresses: ekomasoveg@gmail.com (E.G. Ekomasov), bgu@bk.ru (A.M. Gumerov), xc.89@mail.ru (R.V. Kudryavtsev).URL: <http://soliton.fizfaka.net> (A.M. Gumerov).

are developed. For example, in paper [9] a compact finite-difference scheme and DIRKN-method are used. The compactness of the first scheme is that its recursive formula for a new temporary layer calculation contains not more than nine template points, including the central node where the derivatives are approximated. DIRKN-method implies a class of “diagonally implicit Runge–Kutta–Nystrom methods”. Paper [10] proposes to solve the MSGE by numerical method using collocation and radial basis functions. The method of lines is used in [11]. A number of studies [12–14] use spectral and pseudospectral Fourier methods for solving equations of the MSGE type. [15] presents “gridless” scheme, using the “multi-square” quasi-interpolation. This method does not require solutions of large-scale systems of linear algebraic equations. In [16,17] there used different variants of methods based on the “predictor–corrector” scheme.

The researchers interest is attracted to the question of various types of disturbances influence on the soliton dynamics (see e.g. [18–21]). Many papers are devoted to the study of the spatial modulation (heterogeneity) of the periodic potential (or presence of impurities in the system) influence on the MSGE solitons dynamics. (see e.g. [1,2,4–8,22,23]). The model of a classical particle for the kink interaction with impurity is applicable in the case when the impurity does not allow the existence of the impurity mode—localized vibrational state on the impurity (see [1,2,4]). The importance of impurity modes for kink dynamics is shown in [1,5–8,22–25].

Here we would like to note the emergence of such an interesting effect, as the reflection of the kink moving by inertia in the dissipation-free environment by an attractive impurity due to resonance energy transfer between translational kink mode and impurity mode. For real physical systems are always characterized by the presence of dissipation, which can fundamentally influence on the system behavior. In this regard, it is necessary to investigate the influence of damping and external force on the resonance effects at MSGE kinks motion of a model with an attractive impurity.

2. Main equations and analytical solution method

The MSGE that is going to be studied in this paper is given by [26–29]:

$$u_{tt} - u_{xx} + \sin u = \varepsilon \delta(x) \sin u - 2h \sin \frac{u}{2} - \alpha u_t, \quad (2)$$

where summand $\varepsilon \delta(x)$ simulates a point impurity, $\delta(x)$ —Dirac delta function, ε —constant, h —parameter that determines the external force amplitude, α —damping constant. Corresponding Lagrangian and Rayleigh dissipative function for Eq. (2):

$$L = \int_{-\infty}^{+\infty} \left\{ \frac{1}{2} u_t^2 - \frac{1}{2} u_x^2 - [1 - \varepsilon \delta(x)] (1 - \cos u) + 4h \cos \frac{u}{2} \right\} dx, \quad (3)$$

$$R = \int_{-\infty}^{+\infty} \frac{1}{2} \alpha u_t^2 dx. \quad (4)$$

In the case of zero right side Eq. (2) becomes the sine-Gordon equation (SGE) and has a solution in the form of a topological soliton (or kink):

$$u_0(x, t) = 4 \arctan [\exp(\pm \gamma (x - x(t)))], \quad (5)$$

where $\gamma = (1 - v^2)^{-1/2}$, v —kink velocity, $x(t) = vt + x_0$ —coordinate of the kink center. If the speed is low ($v \ll 1$), then $\gamma \approx 1$. Solving the linearized for small u SGE one can find an expression that describes the structure of the impurity mode:

$$u_1(x, t) = a(t) e^{-\varepsilon|x|/2}, \quad (6)$$

where $a(t) = a_0 \cos(\Omega t + \theta_0)$, Ω —the impurity mode frequency (11), and θ_0 —the initial phase.

The case of a single point impurity excluding external power and dampening has been previously studied in detail (see [1,2,5,6]). It was shown that in the case of “non-deformable kink” approach the impurity acts as a potential. Moreover, for the corresponding sign of the constant ε it acts on kink as an attractive potential, so that a soliton can be localized. For the “deformable kink” approach the effects with a resonant character occur. The possibility of impurity mode excitation on the kink scattering, resulting in a significant change of the kink dynamics results, was also taken into account. For the case of a space extended impurity the interaction of a kink with the impurity for both deformable and non-deformable kink model was also analytically and numerically studied (see [7,22–24,29–32]).

Let’s consider an approximate analytical solution of the Eq. (2) by the collective variables method [1,2]. As a collective coordinates let’s take the coordinate of the kink center $x(t)$ and the amplitude of the impurity mode $a(t)$. Ansatz is the sum of the kink solutions (5) and the impurity mode (6):

$$u = u_0 + u_1 = 4 \arctan e^{x-x(t)} + a(t) e^{-\varepsilon|x|/2}. \quad (7)$$

We assume that $v = \dot{x}(t)$, $a(t)$ and $\dot{a}(t)$ are quite small (value of the order ε). In the framework of this approach $u_1 \ll u_0$. Let's substitute the ansatz (7) in the Lagrangian (3), and after integrating we obtain the following expression:

$$\begin{aligned}
 L_{\text{eff}} \approx & -8 + 4\dot{x}^2(t) + \frac{\dot{a}^2(t)}{\varepsilon} - 2\dot{x}(t)\dot{a}(t) \int_{-\infty}^{+\infty} \frac{e^{-\varepsilon|x|/2}}{\cosh(x-x(t))} dx \\
 & + \frac{2\varepsilon}{\cosh^2(x(t))} + a(t) \frac{2\varepsilon \sinh(x(t))}{\cosh^2(x(t))} + a^2(t) \left[\frac{\varepsilon}{4} - \frac{1}{\varepsilon} - \frac{\varepsilon}{\cosh^2(x(t))} \right] \\
 & + a(t) \int_{-\infty}^{+\infty} \left[\varepsilon \frac{x}{|x|} - 2h + 2 \tanh(x-x(t)) \right] \frac{e^{-\varepsilon|x|/2}}{\cosh(x-x(t))} dx \\
 & + a^2(t) \int_{-\infty}^{+\infty} \left[\frac{1}{\cosh(x-x(t))} + \frac{h}{2} \sinh(x-x(t)) \right] \frac{e^{-\varepsilon|x|}}{\cosh(x-x(t))} dx \\
 & - 4h \int_{-\infty}^{+\infty} \tanh(x-x(t)) dx.
 \end{aligned} \tag{8}$$

In addition $\cos u$ and $\cos \frac{u}{2}$ were expanded in a Taylor to second order terms in ε (an in $a(t)$). Since the resulting Lagrangian (8) is quite complicated to study, let's carry out its simplification. For example, we will not further take into account the terms from the Lagrangian (8) containing integrals of the form

$$\int_{-\infty}^{+\infty} \frac{e^{-\varepsilon|x|/2}}{\cosh(x-x(t))} dx, \tag{9}$$

as they are small everywhere, except for the points $x(t) \rightarrow 0$, because they contain the product of two localized functions. In addition, some summands include factors of the order ε^2 smallness (see [2]). This can greatly simplify the Lagrangian (8) and bring it to the form:

$$\begin{aligned}
 L_{\text{eff}} \approx & -8 + 4\dot{x}^2(t) + \frac{\dot{a}^2(t)}{\varepsilon} - U(x(t)) - a(t)F(x(t)) \\
 & + a^2(t) \left[-\frac{\Omega^2}{\varepsilon} + \frac{1}{2}U(x(t)) \right] - 4h \int_{-\infty}^{+\infty} \tanh(x-x(t)) dx,
 \end{aligned} \tag{10}$$

where

$$\Omega = \sqrt{1 - \varepsilon^2/4}, \tag{11}$$

$$F(x(t)) = -\frac{2\varepsilon \sinh(x(t))}{\cosh^2(x(t))}, \tag{12}$$

$$U(X) = -\frac{2\varepsilon}{\cosh^2(x(t))}. \tag{13}$$

Similarly, dropping small terms, let's calculate and simplify Rayleigh function (4):

$$\begin{aligned}
 R_{\text{eff}} &= \alpha \left[4\dot{x}^2(t) - 2\dot{x}(t)\dot{a}(t) \int_{-\infty}^{+\infty} \frac{e^{-\varepsilon|x|/2}}{\cosh(x-x(t))} dx + \frac{\dot{a}^2(t)}{\varepsilon} \right] \\
 &\approx \alpha \left[4\dot{x}^2(t) + \frac{\dot{a}^2(t)}{\varepsilon} \right].
 \end{aligned} \tag{14}$$

Earlier in the dissipation-free case it has already been shown that a similar simplified model can qualitatively describe a number of interesting phenomena (such as, for example, a resonant energy exchange between a kink and impurity mode).

Substitution of these expressions (10) and (14) in the Euler–Lagrange equation of the second kind for the effective coordinates $x(t)$ and $a(t)$ and truncation of the terms of the order ε^3 leads to the motion equations in the form of:

$$8[\ddot{x}(t) + \alpha\dot{x}(t) - h] + U'(x(t)) + a(t)F'(x(t)) = 0, \tag{15}$$

$$\ddot{a}(t) + \alpha\dot{a}(t) + a(t)\Omega^2 + \frac{\varepsilon}{2}F(x(t)) = 0. \tag{16}$$

If we compare the resulting system of differential equations (15)–(16) with a similar system (see [1,2,6]), obtained for the dissipation-free case in the absence of an external force, it is clear that the inclusion of damping and external force led to addition of summands $8[\alpha\dot{x}(t) - h]$ in the first equation and $\alpha\dot{a}(t)$ in the second equation. Moreover, the impact of the external force on the impurity as a summand of the third order of smallness in this approach is not considered.

Let us analyze the dynamics of a kink obeying Eqs. (15)–(16). Fig. 1 shows the time dependence of the kink center coordinate $x(t)$, calculated by integrating the system of Eqs. (15)–(16) for different cases. In this model the kink initial

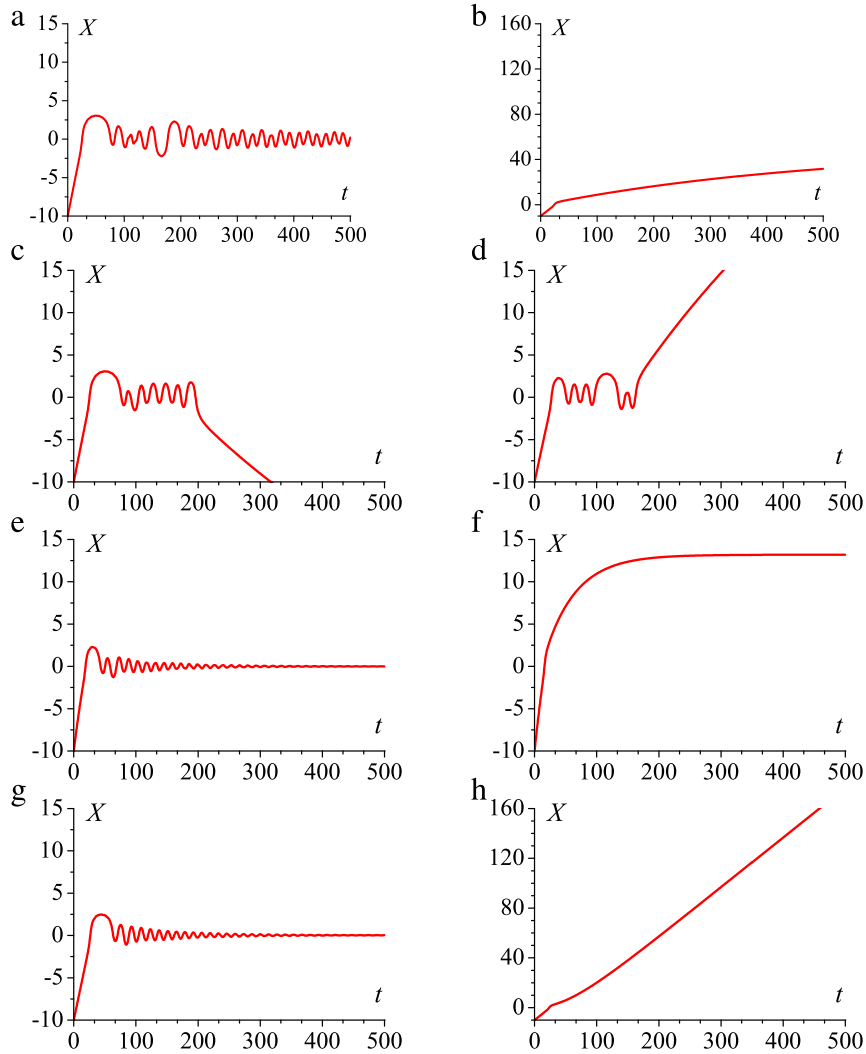


Fig. 1. The dependence of the kink center coordinates $x(t)$ on time, acquired as a result of system simulation (15)–(16) during the motion of the kink by inertia (a, b, c, d, e, f) and under the influence of an external force h (g, h). Simulation parameters $\varepsilon = 0.7, x(0) = -10, a(0) = 0, \dot{a}(0) = 0$: (a) $\alpha = 0.002, h = 0, \dot{x}(0) = 0.3768$; (b) $\alpha = 0.002, h = 0, \dot{x}(0) = 0.4$; (c) $\alpha = 0.002, h = 0, \dot{x}(0) = 0.377$; (d) $\alpha = 0.002, h = 0, \dot{x}(0) = 0.3486$; (e) $\alpha = 0.02, h = 0, \dot{x}(0) = 0.6$; (f) $\alpha = 0.02, h = 0, \dot{x}(0) = 0.7$; (g) $\alpha = 0.02, h = 0.007, \dot{x}(0) = 0.35$; (h) $\alpha = 0.02, h = 0.008, \dot{x}(0) = 0.4$.

energy E_{kink}^0 and work of external force E_{ex} , besides the cost on the impurity mode E_{im} excitation, are spent on the damping in the system E_α :

$$E_{kink}^0 + E_{ex} = E_{kink} + E_{im} + E_\alpha. \tag{17}$$

Therefore, at inertial motion kink does not go to infinity, but stops after a while. This is seen from Fig. 1(b), built with weak damping $\alpha = 0.002$, and Fig. 1(f)—with a stronger damping $\alpha = 0.02$. If the system is influenced by an external force $h > 0$ and dissipative losses E_α are compensated by the energy influx E_{ex} , then the kink may go to infinity if its kinetic energy turns out to be large enough to overcome the impurity attractive potential (see Fig. 1(h)).

The results showed that for the system (15)–(16) as well as for the dissipation-free case, the kink resonant interaction with impurity mode is typical. As a result of interaction the kink may even after repeated impurity crossing leave its attractive potential. However, these evolution variants are found only at low damping and kink motion by inertia. For example, Fig. 1(c) (built at $\alpha = 0.002$), the kink is reflected in the opposite direction after fourteen, and in Fig. 1(d)—in forward direction after eleven impurity crossings. At a stronger damping (e.g. $\alpha = 0.02$) similar evolution variants were not found. Furthermore, a kink may be captured by an attractive potential of impurity, wherein the amplitude of its translational vibrations decreases sufficiently rapidly, as shown in Fig. 1(e). Accounting the impact of external force h does not lead to the appearance of kink resonant reflections. Fig. 1(g) is a case of pinning at $\alpha = 0.02$ and $h = 0.007$, that does not fundamentally differ from the case when $h = 0$ (Fig. 1(e)).

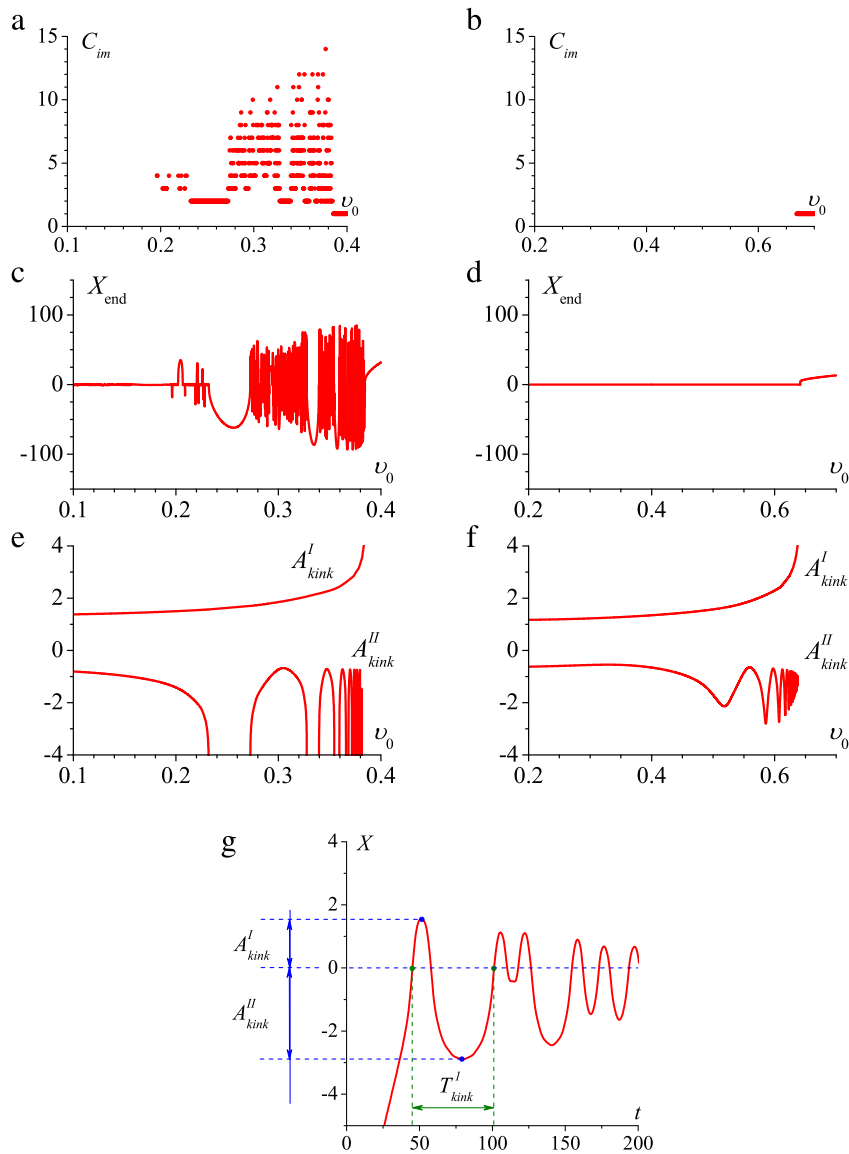


Fig. 2. The number of the kink crossings the impurity C_{im} (a, b), the final position of the kink $x_{end} = x(t_{end})$ (c, d), the value of the maximum A_{kink}^I and minimum A_{kink}^{II} kink translational oscillations (e, f) depending on the kink initial (stationary) speed v_0 in the model (15)–(16), where $\varepsilon = 0.7$, $x(0) = -10$, $a(0) = 0$, $\dot{a}(0) = 0$. When constructing the parameter v_0 was tabulated with step $\delta v = 10^{-4}$: at: (a, c, e)– $\alpha = 0.002$, (b, d, f)– $\alpha = 0.02$. For (c, d) cases $x_{end} < 0$ correspond to the kink reflection from the impurity, $x_{end} > 0$ –kink passing through the impurity, $x_{end} = 0$ –kink capture in the impurity. (g) shows the definition of the maximum A_{kink}^I and minimum A_{kink}^{II} , where T_{kink}^I –is the first period of the kink oscillations in the impurity.

A more complete picture of the kink-impurity interactions is presented in Fig. 2(a) (for weak damping $\alpha = 0.002$) and in Fig. 2(b) (for strong damping $\alpha = 0.02$). They show the dependence of the number of impurity crossings C_{im} from the initial steady-state kink speed v_0 . The comparison to the same curve for the dissipation-free case shows that the appearance of weak damping in the system significantly reduces the number of resonance windows and value C_{im} . And strong damping leads to the virtual disappearance of resonances.

Note that in the study of the resonance windows the reflections lose relevance dependences $v_{kon}(v_0)$ curves (see, [1,6,7, 23,30]), since the final velocity of the kink in the long-term modeling is either equals zero (inertial motion), or equals $v_{st}(h)$ (in the case of movement under the external force influence). Therefore, it is now necessary to use the curves of the kink final position $x_{end} = x(t_{end})$ dependence on v_0 shown in Fig. 2(c), (d). The comparison of these dependences also suggests that with the emergence of weak damping the number of resonance windows is also beginning to decline, especially at small v_0 . This phenomenon can be explained by analyzing the dependence of the translational oscillations amplitude minimum A_{kink}^{II} (which is defined as shown in Fig. 2(g)) on v_0 shown in Fig. 2(e), (f). This dependence shows that wide windows ($C_{im} = 2$) under weak damping (Fig. 2(e)) become small minimums with strong damping (Fig. 2(f)). This suggests that the resonant

interaction between a kink and impurity mode is still the case, but the losses in the system do not leave the kink enough energy to leave the impurity attractive potential. Thus, additional channels of the damping of different type (waves radiation or system dissipation) weaken the effects resulting from the resonant interaction of a kink and impurity mode.

3. Numerical method

For the numerical solution of Eq. (2) let's use the method of finite differences, which produces a grid function U_h whose values are approximately equal to the exact solution U at grid points. There was selected a three-layer explicit solution scheme, with the derivatives approximation on the five-point pattern of “cross” type that was previously used for other SGE modifications (see [29,30]). In the framework of this method, the solution of Eq. (2) is reduced to computing the sought function at given grid nodes with the help of the recurrences

$$U_i^{n+1} = C_2 (U_{i-1}^n + U_{i+1}^n) + C_3 U_i^n + C_4 U_i^{n-1} - K^*(x) \sin U_i^n - C_h \sin 0.5 U_i^n, \tag{18}$$

where

$$C_1 = \left(\frac{1}{\Delta t^2} + \frac{\alpha}{2\Delta t} \right)^{-1}, \quad C_2 = \frac{C_1}{\Delta x^2}, \quad C_3 = C_1 \left(\frac{2}{\Delta t^2} - \frac{2}{\Delta x^2} \right), \tag{19}$$

$$C_4 = C_1 \left(-\frac{1}{\Delta t^2} + \frac{\alpha}{2\Delta t} \right), \quad K^*(x) = C_1(1 - \varepsilon\delta(x)), \quad C_h = 2C_1 h.$$

Here, Δx is the spatial mesh size and Δt is the time step. Introducing the function $K^*(x)$, we can compute it prior to the simulation, thus eliminating few arithmetic operations at every step. Numerical scheme (18)–(19) is stable if $(\Delta t / \Delta x)^2 < 1$. A kink of form (5) moving at the constant velocity v_0 was specified as an initial condition, and the boundary conditions were $U(-\infty, t) = 0, U(+\infty, t) = 2\pi, U'(\pm\infty, t) = 0$.

The typical implementations of the numerical solution to Eq. (2), used in our earlier works (for example, [33,34]), make it possible to calculate the structure and dynamics of kinks with accuracy sufficient for observing the pinning of a kink by an impurity, its passage through an impurity, and the structure and properties of excited nonlinear waves. However, higher numerical accuracy is required for the study of possible resonance effects. For this reason, the function $U(x, t)$ was approximated using $N_x = 10^4$ points.

4. Numerical experiments

4.1. Implementation and numerical optimization

Scheme (18)–(19) was numerically implemented in Delphi. Additionally, the algorithm was optimized to reduce the CPU time. Specifically, by using the specific properties of the problem and reducing the numerical accuracy and the range of the argument, the computation of the sine function was accelerated by more than eight times with the help of the polynomial approximation

$$\sin x \approx -4B(x) [1 + B^2(x) [A_3 + B^2(x) [A_5 + B^2(x) [A_7 + B^2(x) [A_9 + B^2(x)A_{11}]]]]] \tag{20}$$

$$B(x) = 0.25x + \pi/4, \quad A_7 = -0.79794217405921,$$

$$A_3 = -2.66592780638819, \quad A_9 = 0.16264977471553,$$

$$A_5 = 2.12775693434532, \quad A_{11} = -0.01573479830529.$$

With the use of approximate formula (20), the sine on the interval $[2, 8]$ can be computed to 10^{-4} accuracy. The condition for finding the argument of the sine in this interval is ensured by monitoring the residual and the total energy of the system.

To optimize memory access operations, we used the built in assembler of the Delphi compiler. As a result, rejecting the high level programming language, we overcame many of its restrictions and produced a much more optimal code than that generated by the compiler. Tests showed that the overall acceleration of the computations due to the optimization performed was roughly 5.5 times as compared with the conventional implementation (for example, [33,34]). Since the achieved performance came very close to the scheme performance theoretical rating, the need to use different mathematical libraries accelerating calculations (e.g., ACLM and MKL) is eliminated. It should also be noted that the constructed schemes have possibility for further computational optimization via paralleling by special CPU instruction sets (SSE, FMA, AVX) [35–37].

Many conducted optimizations would have a weaker effect while using the implicit scheme for the construction of equations finite-difference approximations, as an implicit scheme is two-step as a rule and requires a larger number of memory accesses. For example, one-dimensional case usually requires a seven- or nine-points scheme [38,39], which, although they have less strict stability conditions, require more time to calculate each new point. The same applies to a four-point scheme of “leapfrog” type [38], because it requires calculation of the trigonometric function in two points. Furthermore, the implicit scheme reduces arithmetic operations density, even for a one-dimensional

case, as it requires an intermediate row of running coefficients computation. This fact becomes even more evident when trying to use further possibilities for optimization, when the paralleling goes in data (within one temporal layer). Furthermore, implicit scheme leads to a considerable complication of iterative schemes for two-dimensional and especially three-dimensional cases (due to necessity to perform intermediate calculations between temporal layers). The scheme used is convenient because it can be with minimal changes adapted both for other modifications of one-dimensional Eq. (2), and for SGE multi-dimensional variants (including methods of optimization).

4.2. Suppression of waves reflection

As shown by numerical simulation, there is an effect of waves reflection from the edge of the grid, that distorts the results obtained after prolonged process modeling. For the “absorption” of the waves in the border region there developed many methods [40,41], including for wave equations of the second order [42]. For Eq. (2) there is a method in which the dissipative parameter α is specified in a piecewise constant functions:

$$\alpha = \begin{cases} 1, & x \leq x_{\text{left}} + D_{\text{diss}}, \quad x \geq x_{\text{right}} - D_{\text{diss}} \\ \alpha_0, & x_{\text{left}} + D_{\text{diss}} < x < x_{\text{right}} - D_{\text{diss}}, \end{cases} \quad (21)$$

where D_{diss} – the absorption region width (typically 3%–5% of the entire simulated field width), α_0 – the value of the dissipative parameter in the main area. Usage of (21) leads to an almost complete damping of all waves advancing to the edges of the grid.

4.3. Numerical error

To estimate the error of the method a comparison of the calculation results $\theta(x_i, t_n)$ for fixed x_i , while changing t_k , using Eq. (2) with its exact solution (5) (when $\varepsilon = 0, h = \alpha = 0$) was made. Absolute error can be calculated by the formula:

$$\Delta\theta = \left| \theta_{i,j}^n - 2 \arctan [\exp(\gamma(x_i - vt_k))] \right|, \quad (22)$$

and reduced error can be calculated by the formula:

$$\varepsilon = \frac{\Delta\theta}{X_n}, \quad (23)$$

where X_n —normalized value, determined as equal to the upper limit of measurements, in this case $X_n = \pi$. Numerical simulation showed that there is an accumulation of errors over time, but the rate of its growth is quite slow. Even with large values $t = 500$ the error is $\varepsilon \approx 0.0125\%$.

4.4. Two schemes of numerical experiment

It is well known (see [1,2]), that under the influence of external force h an initially resting kink in a homogeneous dissipative medium is accelerated to a stationary velocity

$$v_{st} = \frac{h}{\alpha\sqrt{1 + h^2/\alpha^2}}, \quad (24)$$

for some time t_{st} . Fig. 3(a) shows the dependence of kink velocity $v(t)$ on time. The curve 1 shows that $v(t)$ asymptotically approaches to $v_{st}(h = 0.015) = 0.6$. To study the effect of dissipation and external force on the dynamics of a kink at crossing the impurity region we use two schemes of numerical experiment. The first scheme of the experiment suggests that the resting at the initial time kink accelerates to a velocity close to stationary, and then crosses the impurity. Relevant to this case dependence of the kink velocity (Fig. 3(a), curve 2) shows that, after crossing the center of the impurity at the time $t^* \approx 240$ the kink speed drops significantly, but then again asymptotically approaches to the value v_{st} . Meanwhile the dependence $x(t)$ (Fig. 3(c), the curve 2) slightly differs from the case when the impurity is absent (Fig. 3(c), curve 1).

The second scheme of the experiment allows us to study the damping effect without external force. At first, the kink by an external force reaches a velocity close to stationary. This comes at time t_{off} when the kink is in the point $x^* - 10$, where x^* —impurity center (Fig. 3(d)). At this point, external power is turned off, and further movement of the kink occurs by inertia. The corresponding dependence of the kink velocity on time is shown in Fig. 3(b) (curve 1), which suggests that the kink velocity under the decay effect is gradually reduced to zero and after a certain time the kink stops at a certain point (Fig. 3(d), curve 1). Fig. 3(b), (d) (curve 2) shows that in the presence of impurity the kink velocity decreases faster, and the final point at which the kink stops is much closer to the impurity.

Note that the acceleration of the kink to the stationary velocity requires large simulation time, which is generally limited by computing resources. For example, in the cases of Fig. 3(a), (b), the time of meeting the stationary velocity is reduced to

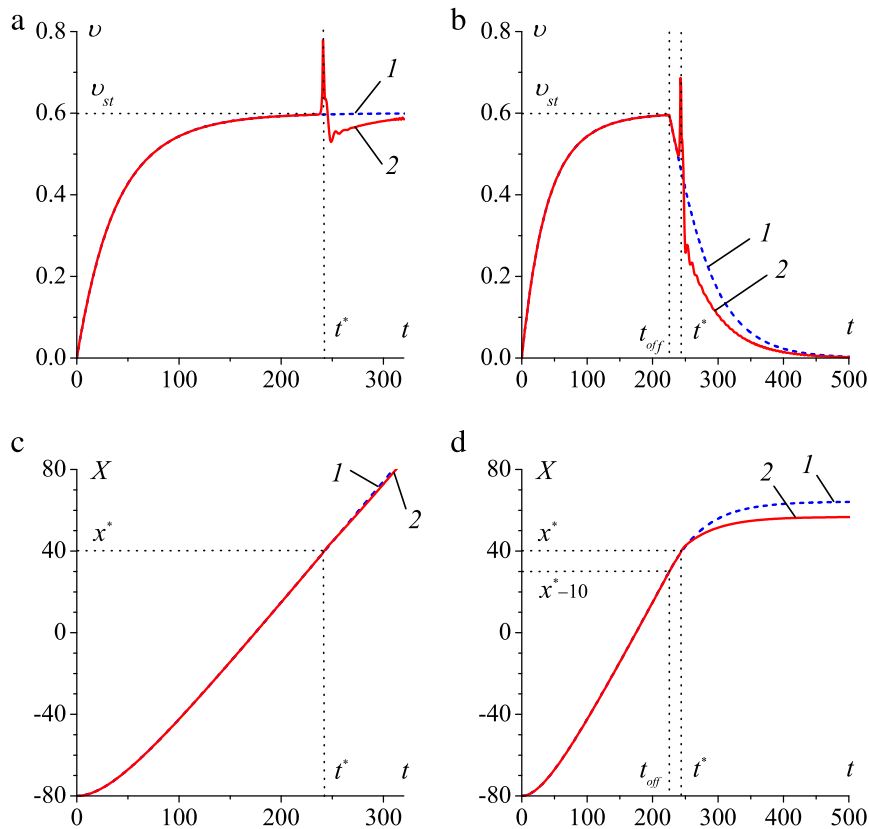


Fig. 3. The kink velocity v (a, b) and its position x (c, d) depending on time t by the action of the external force $h = 0.015$ and the damping $\alpha = 0.001$. In cases (b, d) external power is turned off at the time $t_{off} = 225$ and the kink continues to move by inertia. Curve 1 is plotted for the case when the impurity is absent, curve 2—the case when the kink crosses the impurity center $x^* = 40$, at $\varepsilon = 0.7$ and time t^* . $v_{st}(h) = 0.6$ —the kink stationary velocity.

a value $t_{st} = 225$, at which the kink acquires the velocity $v(t_{st}) \approx 0.5956$. However, the numerical experiment allows to reduce the time of meeting the stationary velocity to $t_{st} = 15$ if at the initial time of simulation the kink velocity v_0 is given by the formula (24). Thus we get the kink velocity much closer to the stationary: $|v(t_{st}) - v_{st}| \approx 10^{-5}$.

Since all further results are conducted in accordance with the described experiment schemes, where the kink is initially accelerated to a stationary velocity by an external force h , so the initial velocity of the kink v_0 is the velocity the kink steady motion, common to the given α and h : $v_0 = v_0(h, \alpha) = v_{st}(h, \alpha)$. The calculated dependences of the sought values of h on the graphs are easier to build depending on v_0 , since, according to (24), the same value h has different effect on the system when different α , which in turn leads to difficulties when comparing the graphs, calculated for different values of damping α .

4.5. Comparison of the analytical model to numerical results

Let's compare the results obtained by using the analytical model (15)–(16) with the numerical results of the original Eq. (2). Let us first consider the simplest case of a kink motion in the absence of impurity. If the external force is absent, the kink after starting to move at velocity v_0 under the influence of the damping will begin to move with negative acceleration until it stops at a certain point. Fig. 4 shows time evolution of the coordinates of the kink center for three different values v_0 . It is seen that the dependences $x(t)$ for the original Eq. (2) (indicated by solid lines) qualitatively agree with the dependences for the model (15)–(16) (indicated by dots). At small values v_0 there is also found a quantitative agreement (see. Fig. 4, curve 3).

Next let's consider the kink motion, which rests at the initial time under the influence of an external force h . Fig. 5 shows the velocity of kink motion depending on time for three different values of the parameter h . This figure suggests that after a certain time the kink velocity reaches a certain stationary value $v_{st} = v_{st}(h, \alpha)$. For the model (2), the value is determined by the expression (24). For the analytical model, as the quasirelativistic effects were not taken into account, the stationary condition leads to the equation $\alpha \dot{x}(t) - h = 0$ and the following expression:

$$v_{st} = \dot{x}(t) = \frac{h}{\alpha}. \tag{25}$$

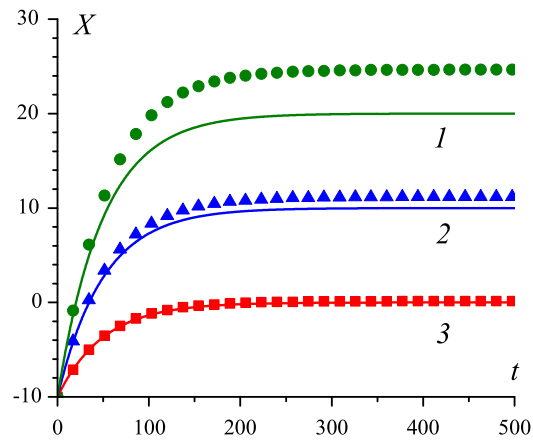


Fig. 4. The dependence of the kink center coordinates x on time t calculated in the framework of models (15)–(16) (solid lines) and (2) (points), where $h = \varepsilon = 0$, $\alpha = 0.02$, $x(0) = -10$, $a(0) = 0$, $\dot{a}(0) = 0$: (1) $v_0 = 0.6$, (2) $v_0 = 0.4$, (3) $v_0 = 0.2$.

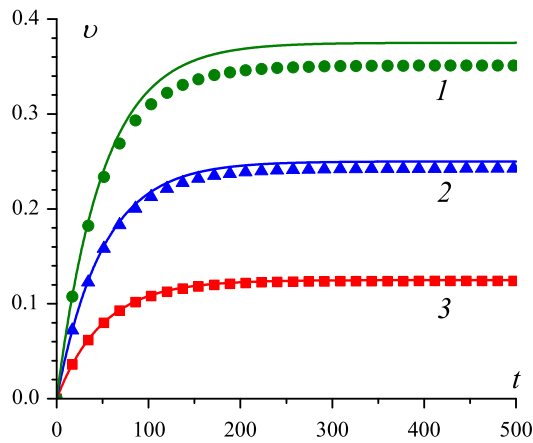


Fig. 5. The dependence of the kink center coordinates x on time t calculated in the framework of models (15)–(16) (solid lines) and (2) (points), where $\varepsilon = 0$, $\alpha = 0.02$, $x(0) = -10$, $a(0) = 0$, $\dot{a}(0) = 0$, $v_0 = \dot{x}(0) = 0$: (1) $h = 0.0075$, (2) $h = 0.0050$, (3) $h = 0.0025$.

Thus, the comparison of the results of the analytical and numerical models shows their qualitative agreement, see, e.g., Fig. 4. Good quantitative agreement is observed only for small values h . Such behavior can be explained by the fact that when choosing a test function for the model (15)–(16) the quasirelativistic effects were not taken into account.

Let's consider the effect of damping on the appearance of the kink-impurity resonance interactions. Fig. 6(a), (b) show the dependence of the maximum A_{kink}^I and minimum A_{kink}^{II} translational vibrations of the kink moving by inertia (which are defined as shown in Fig. 2(g)) on the initial kink stationary velocity v_0 , which show that there is a situation similar to Fig. 2(f). Moreover, even slight damping ($\alpha = 0.002$ in Fig. 6(a)) leads to the disappearance of the reflection resonant windows. This can be explained by the fact that compared to the analytical model while fulfilling the numerical calculation, in addition to damping, there is still an additional damping channel in the form of waves radiation at the kink interaction with the impurity mode. This leads to significant kink energy losses even with little damping. As shown in [30], this damping channel can be compared to the usual one at $\alpha = 0.02$. At stronger damping ($\alpha = 0.02$ in Fig. 6(b)) the amplitude of the kink translational oscillations noticeably reduces. Enabling constant external force (see. Fig. 6(c)) further weakens the effect of resonant interactions and the amplitude of the kink translational oscillations becomes smaller than for the case in Fig. 6(b), as the external force prevents the kink moving in the opposite direction (with fluctuations in the impurity region).

5. Conclusion

In the paper the dynamics of the sine-Gordon equation kinks scattering on a point impurity with regard to resonant effects occurrence was investigated. Using the method of collective variables, a system of differential equations for the coordinates of the kink center and the impurity wave amplitude, describing the dynamics of the kink scattering in the single spot impurity, is acquired.

A quick highly-precise way of the modified sine-Gordon equation numerical solution with a simple explicit scheme of “cross” type was suggested. The possible methods of calculations optimization were given and their effectiveness was

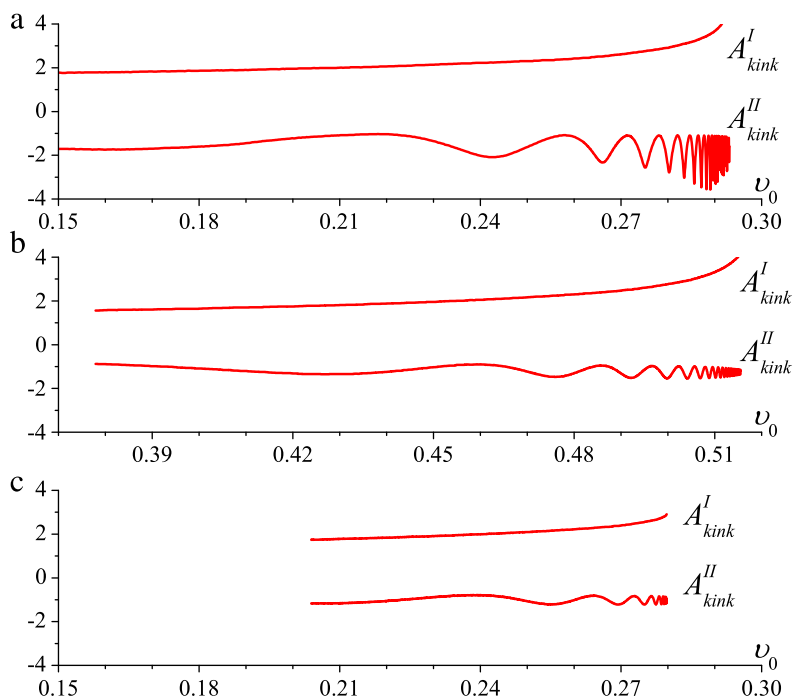


Fig. 6. The value of the maximum A_{kink}^I and minimum A_{kink}^{II} kink translational oscillations depending on the kink initial (stationary) speed v_0 in the model (15)–(16), where $x(0) = -10$, $a(0) = 0$, $\dot{a}(0) = 0$, in the case of the kink motion by inertia (a, b) and under the external force h (c). In the last case $v_0 = v_{st}(h)$. When constructing the parameter v_0 was tabulated with step $\delta v = 3 \cdot 10^{-5}$ where: (a) $\alpha = 0.002$; (b), (c) $\alpha = 0.02$.

discussed. According to these methods testing results there has been achieved total calculations acceleration of about 5.5 times relative to the conventional implementation of such algorithm. When implementing the decision algorithm, an explicit scheme of “cross” type has a number of advantages compared to some known types of implicit schemes. In terms of algorithms execution speed there may be the case when the benefits provided by the solution implicit schemes are fully neutralized by their computational complexity.

Possible scenarios of kink dynamics in the attractive impurities presence was studied. Analytical and numerical methods show that the damping and external force counteract the development of the kink resonant reflection from attracting impurity. However, the underlying cause resonant energy exchange between solitons still exists. It is shown that the typical values of the external force (much less than unity), which are used in computer experiments in this study, do not have a significant impact on the localized waves fluctuations.

References

- [1] O.M. Braun, Y.S. Kivshar, *The Frenkel–Kontorova Model: Concepts, Methods, and Applications*, Springer-Verlag, Berlin, 2004.
- [2] T. Dauxois, M. Peyrard, *Physics of Solitons*, Cambridge University Press, New York, 2010.
- [3] A. Scott (Ed.), *Encyclopedia of Nonlinear Science*, Routledge, New York, 2004.
- [4] J. Cuevas-Maraver, P.G. Kevrekidis, F. Williams (Eds.), *The Sine-Gordon Model and its Applications: From Pendula and Josephson Junctions to Gravity and High-energy Physics*, Vol. 10, Springer, 2014.
- [5] T.I. Belova, A.E. Kudryavtsev, Solitons and their interactions in classical field theory, *Phys. Usp.* 40 (1997) 359–386.
- [6] F. Zhang, Y.S. Kivshar, L. Vázquez, Resonant kink-impurity interactions in the sine-Gordon model, *Phys. Rev. A* 45 (1992) 6019–6030.
- [7] B. Piette, W.J. Zakrzewski, Scattering of sine-Gordon kinks on potential wells, *J. Phys. A* 40 (2007) 5995–6010.
- [8] J.P. Currie, S.E. Trullinger, A.R. Bishop, J.A. Krumhandl, Numerical simulation of sine-Gordon soliton dynamics in the presence of perturbations, *Phys. Rev. B* 15 (1977) 5567–5580.
- [9] A. Mohebbi, M. Dehghan, High-order solution of one-dimensional sine-Gordon equation using compact finite difference and DIRKN methods, *Math. Comput. Modelling* 51 (2010) 537–549.
- [10] M. Dehghan, A. Shokri, A numerical method for one-dimensional nonlinear sine-Gordon equation using collocation and radial basis functions, *Numer. Methods Partial Differential Equations* 24 (2008) 687–698.
- [11] A.G. Bratsos, E.H. Twizell, The solution of the sine-Gordon equation using the method of lines, *Int. J. Comput. Math.* 61 (1996) 271–292.
- [12] G.L. Alfimov, W.A.B. Evans, L. Vázquez, On radial sine-Gordon breathers, *Nonlinearity* 13 (2000) 1657–1680.
- [13] S.P. Popov, Application of the quasi-spectral Fourier method to soliton equations, *Comput. Math. Math. Phys.* 50 (2010) 2064–2070.
- [14] E.G. Ekomasov, R.K. Salimov, On localized long-lived three-dimensional solutions of the nonlinear Klein–Gordon equation with a fractional power potential, *JETP Lett.* 100 (2014) 477–480.
- [15] M. Li-Min, W. Zong-Min, A numerical method for one-dimensional nonlinear sine-Gordon equation using multiquadric quasi-interpolation, *Chin. Phys. B* 18 (2009) 3099.
- [16] A. Bratsos, A numerical method for the one-dimensional sine-Gordon equation, *Numer. Methods Partial Differential Equations* 24 (2008) 833–844.
- [17] A.Q.M. Khaliq, B. Abukhodair, Q. Sheng, M.S. Ismail, A predictor–corrector scheme for the sine-Gordon equation, *Numer. Methods Partial Differential Equations* 16 (2000) 133–146.

- [18] L. Kavitha, E. Parasuraman, D. Gopi, A. Prabhu, R.A. Vicencio, Nonlinear nano-scale localized breather modes in a discrete weak ferromagnetic spin lattice, *J. Magn. Magn. Mater.* 401 (2016) 394–405.
- [19] V.V. Kruglyak, O.Y. Gorobets, Y.I. Gorobets, A.N. Kuchko, Magnetization boundary conditions at a ferromagnetic interface of finite thickness, *J. Phys.: Condens. Matter* 26 (2014) 406001.
- [20] S.P. Popov, Scattering of solitons by dislocations in the modified korteweg de vries–sine–Gordon equation, *Comput. Math. Math. Phys.* 55 (2015) 2014–2024.
- [21] D. Saadatmand, S.V. Dmitriev, P.G. Kevrekidis, High energy density in multisoliton collisions, *Phys. Rev. D* 92 (2015) 056005.
- [22] R.H. Goodman, P.J. Holmes, M.I. Weinstein, Interaction of sine–Gordon kinks with defects: Phase space transport in a two-mode model, *Physica D* 161 (2002) 21–44.
- [23] K. Javidan, Analytical formulation for soliton–potential dynamics, *Phys. Rev. E* 78 (2008) 046607.
- [24] S.P. Popov, Influence of dislocations on kink solutions of the double sine–Gordon equation, *Comput. Math. Math. Phys.* 53 (2013) 1891–1899.
- [25] E.G. Ekomasov, A.M. Gumerov, R.R. Murtazin, Interaction of sine–Gordon solitons in the model with attracting impurities, *Math. Methods Appl. Sci.* (2016).
- [26] E. Zamora-Sillero, N.R. Quintero, F.G. Mertens, Sine–Gordon ratchets with general periodic, additive, and parametric driving forces, *Phys. Rev. E* 76 (2007) 066601.
- [27] A.L. Fabian, R. Kohl, A. Biswas, Perturbation of topological solitons due to sine–Gordon equation and its type, *Commun. Nonlinear Sci. Numer. Simul.* 14 (2009) 1227–1244.
- [28] B.A. Malomed, Dynamics of quasi–one-dimensional kinks in the two-dimensional sine–Gordon model, *Physica D* 52 (1991) 157–170.
- [29] A.M. Gumerov, E.G. Ekomasov, R.R. Murtzin, V.N. Nazarov, Transformation of sine–Gordon solitons in models with variable coefficients and damping, *Comput. Math. Math. Phys.* 55 (2015) 628–637.
- [30] A.M. Gumerov, E.G. Ekomasov, F.K. Zakiryanov, R.V. Kudryavtsev, Structure and properties of four-kink multisolitons of the sine–Gordon equation, *Comput. Math. Math. Phys.* 54 (2014) 491–504.
- [31] E.G. Ekomasov, A.M. Gumerov, R.R. Murtazin, R.V. Kudryavtsev, A.E. Ekomasov, N.N. Abakumova, Resonant dynamics of the domain walls in multilayer ferromagnetic structure, *Solid State Phenom.* 233–234 (2015) 51–54.
- [32] E.G. Ekomasov, A.M. Gumerov, Numerical simulation of the generation of multisoliton type magnetic inhomogeneities in ferromagnets with inhomogeneous parameters, *Lett. Mater.* 4 (2014) 237–240.
- [33] E.G. Ekomasov, S.A. Azamatov, R.R. Murtazin, Studying the nucleation and evolution of magnetic inhomogeneities of the soliton and breather type in magnetic materials with local inhomogeneities of anisotropy, *Phys. Met. Metall.* 105 (2008) 313–321.
- [34] E.G. Ekomasov, S.A. Azamatov, R.R. Murtazin, Excitation of nonlinear solitary flexural waves in a moving domain wall, *Phys. Met. Metall.* 108 (2009) 532–537.
- [35] Amd64 architecture programmer's manual. 128-bit and 256-bit media instructions, *Advanced Micro Devices* 4 (2013).
- [36] Intel® 64 and ia-32 architectures optimization reference manual, Intel Corporation (2013).
- [37] Intel® 64 and ia-32 architectures software developer's manual, Intel Corporation (2013).
- [38] R.K. Dodd, J.C. Eilbeck, J.D. Gibbon, H.C. Morris, *Solitons and Nonlinear Wave Equations*, Academic Press, London, 1982.
- [39] D. Furihata, Finite-difference schemes for nonlinear wave equation that inherit energy conservation property, *J. Comput. Appl. Math.* 134 (2001) 37–57.
- [40] B. Engquist, A. Majda, Radiation boundary conditions for acoustic and elastic wave calculations, *Comm. Pure Appl. Math.* 32 (1979) 313–357.
- [41] A.A. Konstantinov, V.P. Maslov, A.M. Chebotarev, Shift of the boundary conditions for partial differential equations, *USSR Comput. Math. Math. Phys.* 28 (1988) 111–121.
- [42] R.L. Higdon, Numerical absorbing boundary conditions for the wave equation, *Math. Comp.* 49 (1987) 65–90.